CONF-791112--38

IMPLANTATION STUDIES OF IMPURITY IMMOBILIZATION MECHANISMS*

S. M. Myers
Sandia Laboratories†
Albuquerque, NM 87185

Ion-implanted alloys have been used to study mechanisms of impurity immobilization in metals. These phenomena provide a means of suppressing detrimental impurity effects such as embrittlement. Processes investigated include the reaction of Al and Fe in Be to form $AlFeBe_4$ precipitates, the trapping of Sb in Fe by TiC and TaC precipitates, and the binding of hydrogen in Fe to lattice defects and to Y solutes. The broader applicability of the method of investigation is considered in the context of these examples.

*This work supported by the US Department of Energy, DOE, under Contract DE-AC04-76-DP00789.

†A US Department of Energy Facility.

Introduction

Dilute impurities may severely degrade the mechanical properties of alloys, most frequently causing loss of ductility. A notable example is the embrittlement of steels by hydrogen(1) and by the metalloids Sb, Sn, As, and P(2). Such effects often persist for impurity concentrations down to $\sim 10^{-3}$-10^{-5} atomic fraction. Since purification to these levels is costly and sometimes nullified by contamination during service, there is a strong impetus to control embrittlement without excluding the responsible impurities. One means of accomplishing this is to immobilize the embrittling solutes so that they remain dispersed instead of accumulating at potential fracture sites such as grain boundaries and crack tips. In particular, the detrimental species may be incorporated into a stable intermetallic phase, or they may be trapped by precipitates, other solutes, or lattice defects. Because of their effectiveness in suppressing embrittlement, such mechanisms have been extensively investigated in the past decade.

At Sandia Laboratories, processes which reduce impurity mobility are being investigated using ion-implanted alloys. In these studies, the composition-versus-depth profile and defect distribution of a $\lesssim$1μm layer are initially tailored to exhibit the particular effect of interest. The material is then annealed, and its thermal evolution is monitored by such microscopic probes as ion backscattering/channeling and transmission electron microscopy. Resulting data provide information on the mechanism, kinetics, and strength of the impurity binding. This procedure complements more conventional methods in several respects. It permits a high degree of control over composition-versus-depth, so that both the embrittling solute and the entities with which it interacts can be localized to selected depth intervals. Reactions occurring during annealing can then be observed unambiguously in the depth profiles of the constituents. In addition, implantation is capable of introducing any solute to a concentration of several at.%, so that the influence of extraneous impurities on the data is minimized. Furthermore, since the implantation experiments require diffusion lengths of only $\sim$0.1 - 1μm, measurements can be carried out at the lower temperatures where embrittlement is usually manifested and where the processes of mobility reduction are more prominent.

This paper summarizes the implantation studies of several impurity immobilization mechanisms and discusses their significance for alloy development. The general features and broader applicability of the method are also considered in the context of these examples. The first process to be discussed is the interaction of Al and Fe impurities in Be to form $AlFeBe_4$(3,4). Then, TiC and TaC precipitates in Fe are shown to be effective traps for Sb impurities(5). Finally, the trapping of hydrogen in Fe by lattice defects(6) and by Y (yttrium) atoms(7) is analyzed.

$AlFeBe_4$ Formation in Be(Al,Fe)

Commercial grades of Be usually contain the highly insoluble impurities Al and Fe, and the way in which these species precipitate strongly affects the mechanical properties. Aluminum is particularly detrimental because it tends to separate out at grain boundaries during heat treatment, producing a low-melting interface. It has been recognized for some time that precipitation of the fcc phase of nominal composition $AlFeBe_4$ serves to tie up Al within the Be grains(8). However, quantitative information was previously lacking on the composition range and stability of this phase when it is in equilibrium with hcp Be. Since such data are needed for effective control of Al effects, implantation experiments were carried out to evaluate these properties(3,4).

The reaction between Al and Fe in Be was observed by initially implanting these elements to different depths, and then monitoring their depth profiles during annealing. Typical profiles, obtained by 2 MeV ^4He backscattering, are shown in Fig. 1. Depth is expressed here as the total number of atoms per unit area from the surface, which is the quantity obtained from the backscattering analysis. The 0.2μm interval indicated on the figure assumes that the atomic density is equal to that of unalloyed Be. Following the room-temperature implantation, the overall Al-to-Fe atomic ratio was 3, and the two elements were separated in depth as seen in Fig. 1a.

During annealing at 873 K, a portion of the Al migrated to the Fe-rich layer (Fig. 1b), while transmission electron microscopy showed recovery of implantation damage and precipitation of the phases fcc Al and $AlFeBe_4$. Formation of the latter intermetallic was therefore taken to be the driving force for the Al redistribution. As annealing continued, the Al-Fe reaction eventually reached completion and stopped, leaving excess Al in the deeper peak. The profile after 8 hours given in Fig. 1b reflects such a saturated condition. At this point the Al-to-Fe atomic ratio in the $AlFeBe_4$ phase is assumed to be maximized under the constraint of equilibrium between $AlFeBe_4$ and hcp Be. This ratio is obtained by evaluating the areas under the overlapping Fe and Al peaks. The result $([Al]/[Fe])_{max.} = 1.4$ was obtained

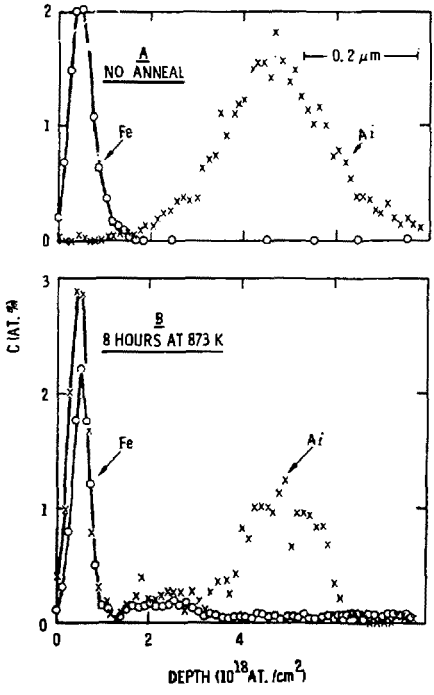

Fig. 1 - Reaction of Al and Fe in Be at 873 K to form $AlFeBe_4$.

over the temperature range 773-1073 K. Similar experiments employing an initial excess of Fe rather than Al yielded $([Al]/[Fe])_{min.} = 0.9$ over the range 773-873 K.

Implantation experiments also provide information on the stability of $AlFeBe_4$ in Be. At a qualitative level, this ternary compound was found to precipitate preferentially over both Al and hcp-$FeBe_{11}$ in the temperature range investigated, 773-1123 K; the latter two phases were observed only when the overall Al-to-Fe ratio was outside the boundaries determined above, resulting in an excess of either Al or Fe. More quantitatively, the heat of precipitation of $AlFeBe_4$ in Be(Al,Fe) can be estimated from the solubilities of Al and Fe in Be when the ternary phase is present: the smaller the solubilities, the greater the heat of formation. Ion-implanted alloys were used to determine these two solubilities at 873, 1073, and 1123 K under conditions where the $AlFeBe_4$ was at its Al-rich extreme. The experiments entailed measuring the concentrations at which Al and Fe diffused from the high-concentration, precipitated layer into the underlying single-phase Be. The solubility values obtained were consistently less than the experimental resolution, 0.02 at.% for Al and 0.01 at.% for Fe. Application of dilute-solution theory(9) to these results yields a heat of precipitation of >0.6 eV per Al or Fe atom incorporated into $AlFeBe_4$. (This estimate assumes that the entropy of precipitation is not very different from the values measured for $FeBe_{11}$ and $CuBe_3$ formation in Be(10).)

The above findings provide significant new information for controlling Al in Be via $AlFeBe_4$ precipitation. For instance, they indicate that Al uptake by this phase stops at $[Al]/[Fe] = 1.4$. In addition, they allow an upper bound to be placed on the concentration of Al remaining in solution as a function of temperature when $AlFeBe_4$ is present. At 1123 K this concentration was determined to be <0.02 at.%. Accepting the prediction of dilute solution theory(9) that the solubility varies as $\exp(-\Delta H/kT)$, where ΔH is the heat of precipitation shown above to be >0.6 eV, one has

$$\text{Al conc.} < (10\text{at.}\%)\exp\left(-\frac{6960\ \text{K}}{T}\right) \qquad (1)$$

At 773 K, for example, this yields an upper bound of 0.0012 at.% Al in the Be phase.

Trapping of Sb by Carbide Precipitates in Fe

Ferritic (bcc) steels frequently contain the metalloids Sb, Sn, As, and P as dilute impurities. If such an alloy is exposed to temperatures in the approximate range 600 - 900 K during fabrication or service, these species tend to segregate at grain boundaries. (Above ~900 K the driving force for segregation is usually weak, whereas below ~600 K the kinetics are very slow.) The result of segregation is believed to be a weakening of intergranular cohesion, producing what is classically referred to as temper embrittlement(2). In seeking to control this widely encountered effect, it is desirable to identify mechanisms whereby the metalloids can be immobilized within the matrix of the grains. One such process has recently been discovered using ion-implanted alloys: Sb was shown to be trapped by small TiC or TaC precipitates in Fe(5).

Results evidencing an affinity between Sb and TiC precipitates are given in Fig. 2. Initially, Sb and Ti were implanted to different depths in Fe at room temperature; the concentration profiles as measured by 2.6 MeV

^{4}He backscattering are shown on the figure. (The Ti concentrations in Fig. 2 are reduced by a factor of 4 to facilitate comparison with the Sb.) After implantation, the specimen was annealed for 0.5 hours at 873 K. The Ti depth profile did not change observably during this heat treatment; instead, C was gettered from dilute bulk impurities and possibly from the environment to form small TiC precipitates. This gettering was observed by using the deuterium-excited nuclear reaction $^{12}C(d,p)^{13}C$ to detect the C(11). The TiC particles were identified by transmission electron microscopy (TEM) and shown to have a mean size of ~2 nm. Microscopy also indicated that the host Fe lattice recovered from implantation damage during the anneal.

It is seen from Fig. 2 that the Sb redistributed during heating, forming a new peak which conforms to the Ti profile in both depth and width. Since TEM showed only the TiC and bcc-Fe phases, this behavior is taken as direct evidence for binding of Sb at the carbide precipitates. One may reasonably hypothesize that the metalloid occupies the TiC-Fe interface in a fashion similar to its demonstrated accumulation at grain boundaries(2).

The above interpretation is reinforced by examining the annealing behavior of Fe implanted only with Sb. Depth profiles from such an experiment are given in Fig. 3. Here the kind of Sb redistribution seen in Fig. 2

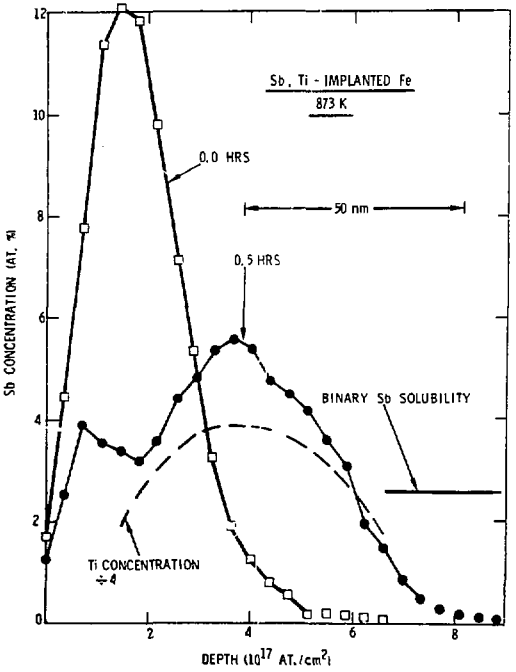

Fig. 2 - Redistribution of Sb to TiC precipitates in Fe at 873 K.

is absent; instead, after annealing, a peak remains at the initial implantation depth. (The obvious reduction in profile area during heat treatment reflects Sb sublimation at the Fe surface. Such loss was greatly reduced in samples also implanted with Ti.) Transmission electron microscopy shows that the region of the Sb peak contains ε-FeSb precipitates, as expected from the equilibrium phase diagram. A diffused tail extends from this precipitated layer into the underlying single-phase Fe, and the two profile structures intersect at 2.65 at.%, which is the Sb solubility at the annealing temperature. This relatively simple behavior is consistent with theoretical expectations for the Fe-Sb binary system. Its observation confirms that the peak shift in Fig. 2 results from implantation of Ti.

When the Sb- and Ti-implanted specimen of Fig. 2 was subsequently annealed for much longer times, a low-concentration Sb tail emerged from the layer containing TiC precipitates. This is seen in Fig. 4, where profiles after 0.5 and 54 hours at 873 K are plotted using an expanded concentration scale. The plateau at 0.23 at.% is the beginning of a tail which

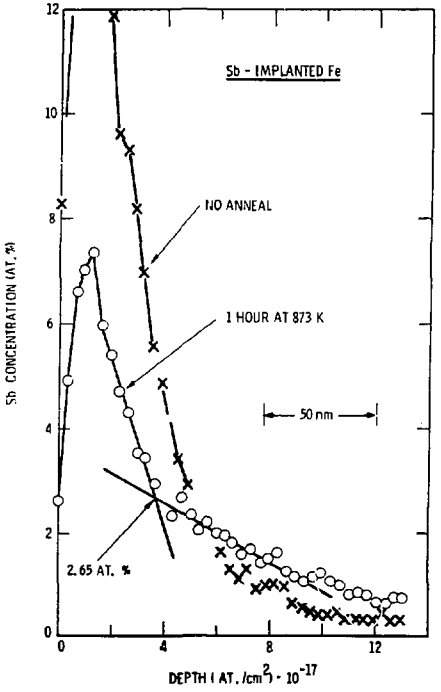

Fig. 3 - Antimony profile evolution at 873 K in Fe not implanted with Ti.

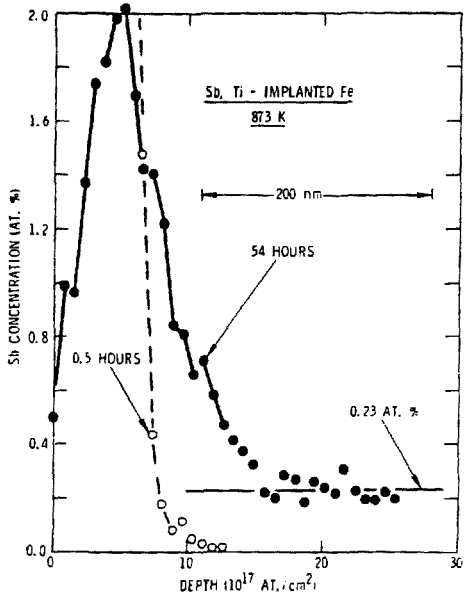

Fig. 4 - Emergence of a diffused Sb tail in the Ti-implanted sample of Fig. 2 after 54 hours at 873 K.

extends to depths much greater than those probed by the ion backscattering analysis. The occurrence of such a peak-and-tail structure is qualitatively reminiscent of the data in Fig. 3 for the binary alloy. However, the concentration level of the tail in Fig. 4, 0.23 at.%, is an order of magnitude smaller than the value observed in Fig. 3, 2.65 at.%. This difference provides further evidence that Sb is bound within the region containing TiC precipitates, and it indicates that the coupling is substantially stronger than that of Sb to the ε-FeSb phase. Finally, behavior similar to that observed in Figs. 2 and 4 was obtained in implantation experiments at 973 K.

As indicated above, it is hypothesized that the trapped Sb occupies the TiC-Fe interface. The interfacial region is assumed to accommodate the large Sb atom more readily than the bcc-Fe lattice. If this interpretation is correct, such trapping might be expected to occur at other second-phase particles. In fact, preliminary experiments indicate that Sb is also bound to TaC precipitates in Fe.

Implantation studies of trapping such as the above may be quantified by mathematically modeling the evolution of the composition-versus-depth profile.

Appending appropriate trapping terms to the diffusion equation yields for the general case(12)

$$\frac{\partial}{\partial t} C_S(x,t) = D \frac{\partial^2 C_S}{\partial x^2} - \sum_i S_i(x,t) \qquad (2)$$

$$\frac{\partial}{\partial t} C_i(x,t) = S_i \qquad (3)$$

where

$$S_i = B_i \left\{ C_S [A_i(x) - C_i] - Z\, C_i \exp\left(-\frac{Q_i}{kT}\right) \right\} . \qquad (4)$$

Here C_S is the concentration of the diffusing species not trapped, C_i is its concentration in traps of type i, and A_i is the density of these traps, all expressed as an atomic fraction of the host phase; A_i is defined so that trap saturation occurs when $C_i = A_i$. The quantities Q_i are the trap binding enthalpies measured with respect to a solutionized site, and Z is the number of solutionized sites per host atom, equal to 1 for substitutional species. The terms S_i take account of the movement of solute between solution and traps. Their evaluation in Eq. 4 may be regarded physically as the difference between two rates: the flow from solution to unoccupied traps, whose concentration is $A_i - C_i$, and the flow from traps to solution. Finally, if the trapping entities (such as precipitates) are separated by distances large compared to their size, and if they may be characterized by an effective spherical radius R_i, then the rate constants B_i are given by(13)

$$B_i = 4\pi R_i D N / \alpha_i \qquad (5)$$

where N is the atomic density of the host phase and α is the number of trap sites per trapping entity. The above system of equations is readily solved by numerical methods(14).

Equations 2 - 5 were applied for conditions approximating an implantation experiment where Sb is trapped by carbide precipitates in Fe at 973 K. A single trap binding enthalpy of $Q_1 = 0.39$ eV was used. Resulting depth profiles of Sb are shown in Fig. 5, where the distribution of traps is given by the dashed line. The theoretical profile after 0.28 hours at 973 K exhibits both the qualitative features of the experimental data emphasized in Figs. 2 and 4, namely, solute redistribution in conformance with the trap distribution and the emergence of a low-amplitude tail.

As a function of anneal time, the above theoretical calculation has the following useful property: after the emergence of the diffused tail, the concentration in this tail just beneath the trapping layer decreases continuously with time, maintaining a nearly constant ratio to the quantity of Sb still trapped. The relation is given by

$$\frac{C_S(\text{tail})}{N \int C_1 dx} = \frac{\exp(-Q_1/kT)}{N \int A_1 dx} \qquad (6)$$

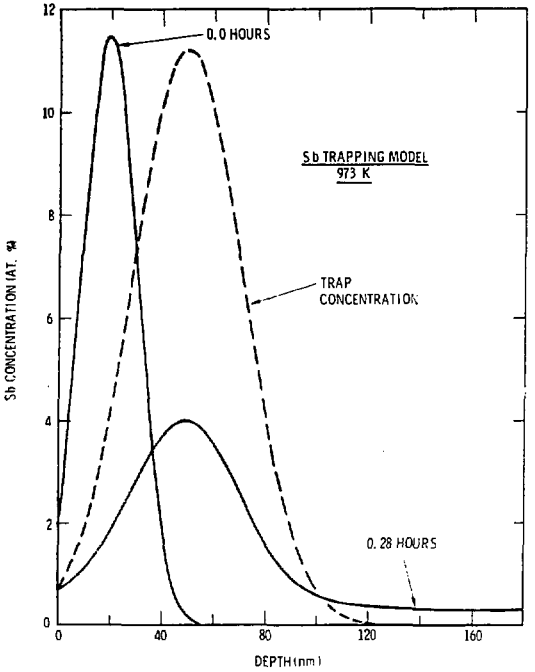

Fig. 5 – Model calculation of the Sb profile evolution at 973 K in the presence of 0.39 eV traps.

where the subscript 1 refers to the single type of trap. This approximation is increasingly accurate as the trap occupancy becomes small compared to one. Physically, Eq. 6 simply states that the fractional occupancies of traps and solutionized sites within a near-surface equilibrated region are related by the Boltzmann factor $\exp(-Q_1/kT)$. This result provides a means of obtaining the trapping enthalpy Q_1, since the total number of traps per unit area $N/A_1 dx$ can be estimated from TEM. Moreover, such a proportional variation is specifically characteristic of trapping, as opposed to incorporation of Sb into an intermetallic phase, so that its experimental observation in the implantation experiments would support the proposed interpretation.

The time-dependent quantities C_S(tail) and $N/C_1 dx$ can be obtained experimentally from backscattering profiles such as the one given in Fig. 4. Data from two isothermal anneal sequences are plotted in Fig. 6, where measurements at shorter times prior to the emergence of the diffused tail are omitted. (Moving to the left on the plot corresponds to increasing the time at temperature.) In one case Ti was implanted to a fluence of 1.0×10^{17} at./cm^2, and the annealing was carried out at 973 K; TEM showed a mean TiC precipitate size of ≈5 nm. The other experiment employed Ta at a lower dose, 1.7×10^{16}

at./cm^2, and the heat treatments were done at 873 K; transmission electron diffraction from this specimen indicated the presence of the TaC phase. Both sets of data are seen to exhibit the proportional variation predicted by Eq. 6. In the case of the TiC experiment, the number of traps per unit area $N\int A_1 dx$ was estimated from the observed precipitate size distribution to be 2.4×10^{16} cm^{-2}. Substituting the slope from Fig. 6 into Eq. 6 then gives a trapping enthalpy of $Q_1 \approx 0.4$ eV.

The implantation experiments discussed above have demonstrated trapping of Sb by small TiC and TaC precipitates in Fe. Consideration of kinetics indicates that this effect should also occur at the much lower Sb densities which typically embrittle steels; indeed, for a fixed temperature and trap density, the fraction of the impurities occupying traps is expected to remain constant down to infinitesimal concentrations. Furthermore, pending experimental confirmation, it seems reasonable to anticipate that the other troublesome metalloids Sn, As, and P will undergo similar trapping, and that the effect is not unique to precipitates of TiC or TaC. For all these reasons, the trapping mechanism identified in the present work appears promising for control of temper embrittlement. To the knowledge of the author, this approach for suppressing metalloid effects in steels had not previously been considered in the literature, nor had the affinity of metalloids for second-phase particles been determined.

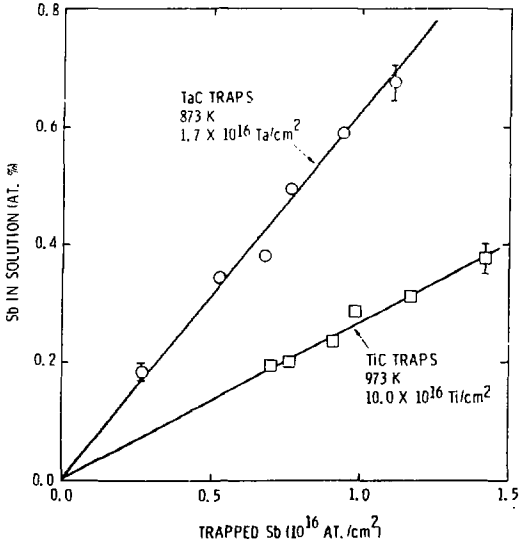

Fig. 6 - Relative variations of the amount of trapped Sb and the Sb concentration in solution for Fe containing TiC or TaC precipitates. Anneal time increases to the left. The error bars indicate the standard statistical error for the solutionized concentration.

Trapping of Hydrogen in Fe

Dilute hydrogen impurities embrittle both ferritic (bcc) and austenitic (fcc) steels(1). Control of this degradation is made difficult by the high hydrogen mobility, particularly in the bcc structure; for example, in pure Fe, $D \sim 10^{-4} cm^2/s$ at room temperature. Such rapid transport allows the impurity to be assimilated from the environment during fabrication or service and to accumulate at grain boundaries or crack tips. Although the specific mechanisms of hydrogen embrittlement remain controversial, there is almost general agreement that suppression of transport is very beneficial. Consequently, trapping processes which accomplish this are of considerable interest. Ion implanted alloys have been used to investigate two such effects in bcc Fe: trapping of hydrogen by defects and by Y (yttrium) atoms.

Trapping by Lattice Defects

The objective of the experiment was to determine how strongly hydrogen is bound to lattice imperfections in Fe and, to the extent possible, characterize the underlying atomic configurations(6). Pure, highly-annealed Fe was initially implanted with the deuterium isotope (D) at a temperature of ≈90 K; a dose of 1.5×10^{16} D/cm^2 was injected at 15 keV, producing a peak concentration of ≈1 at.% at a depth of ≈0.1μm. The implantation also produced extensive lattice damage which served as traps. Subsequently, the specimen temperature was linearly ramped at a rate of 2 K/minute. At 10 K intervals, the amount of D retained within ≈0.4μm of the surface was measured by bombarding with 0.7 MeV ^{3}He and detecting protons from the nuclear reaction $^2D(^3He,p)^4He$. Release from traps was manifested by a decrease in the quantity of D detected, and the temperatures of release were indicative of the trap depths.

The fraction of the initially implanted D remaining within the implanted region is plotted versus temperature in Fig. 7. Two release stages are present, centered at about 260 and 400 K respectively. Other ion beam experiments indicate that the D does not actually leave the sample below 303 K, due to a surface permeation barrier; hence, at least during the 260 K stage, the release occurs primarily into the underlying Fe matrix. Both the stages in Fig. 7 occur at temperatures far too high to be attributed to the onset of perfect-lattice diffusion, and therefore both must be associated with detrapping. It then follows that the ion-damaged region contains at least two distinct defect-trap configurations.

Equations 2 - 5 were employed to model the time evolution of the system. Two different traps were included in the calculation, and their concentrations and binding enthalpies were adjusted to produce agreement with the data. The depth range containing traps was fixed in accordance with the known penetrations of implantation and analysis beams. The results of the model calculation are given in Fig. 7, where agreement between theory and experiment is seen to be excellent. The D trapping enthalpies obtained from the fit are 0.5 eV for the 260 K stage and 0.8 eV for the 400 K stage.

Ion channeling of the ^{3}He analysis beam provided information on the lattice location of the trapped D. Single-crystal Fe was initially implanted at 110 K and then annealed at a series of increasing temperatures. Following the implantation and after each anneal, the specimen was held at 110 K while (100) planar and <100> axial scans were made. Prior to crossing the 260 K stage, the data are consistent with >90% of the D occupying the site shown in Fig. 8; the position is close to high-symmetry octahedral, but displaced by δ=0.04 nm toward a nearest-neighbor substitutional site. After exceeding 260 K, the channeling data changed qualitatively, in a fashion suggesting more

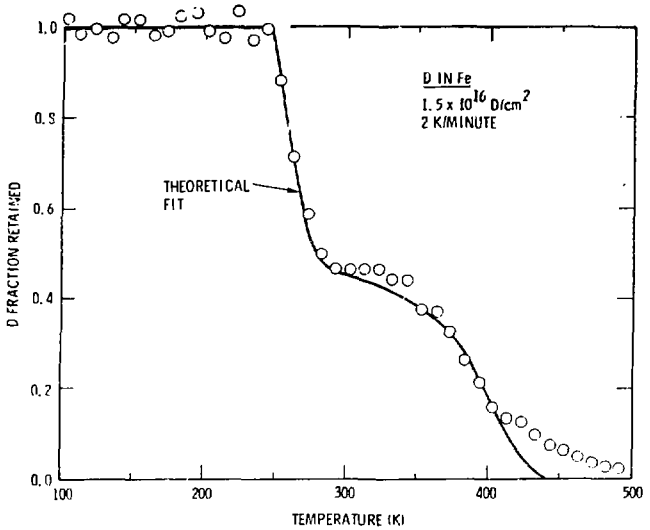

Fig. 7 - *Release of D from defect traps in Fe during linear ramping of* temperature. The solid line is a fitted theoretical calculation with trap depths of 0.48 and 0.81 eV.

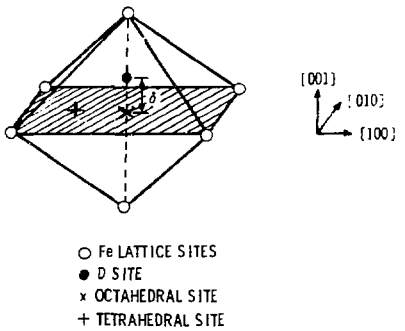

Fig. 8 - Lattice location of D occupying the 0.5 eV defect trap in Fe.

than one D configuration. Consequently, the lattice location shown in Fig. 8 is attributed to the 260 K, 0.5 eV trap. Finally, this experiment did not determine the nature of the defects to which the D is bound. Nevertheless, several considerations suggest that the 0.5 eV traps are vacancies(6). At a more speculative level, vacancy clusters may possibly produce the 0.8 eV trapping.

The 0.5 eV and 0.8 eV defect traps identified in the above implantation experiment greatly reduce the mobility of hydrogen; their binding enthalpies exceed by an order of magnitude the activation enthalpy for diffusion, ≈0.05 eV. Moreover, it seems plausible to suggest that these traps might be introduced on a macroscopic scale by techniques such as cold working. Support for such a view has subsequently come from hydrogen permeation experiments in Fe (15), where cold work delayed the emergence of H_2 gas on the downstream side of the foil. An effective trapping enthalpy of 0.6 eV was deduced, and this lies between the values obtained in the present work. Consequently, defect trapping appears worthy of consideration as one method for controlling hydrogen embrittlement of ferritic steels.

Trapping by Implanted Y

Hydrogen was found to be trapped even more strongly in Fe which had been ion-implanted with Y(7). The experiment was carried out by initially implanting 190 keV Y at room temperature to a dose of 4×10^{16} at./cm^2. Transmission electron microscopy and ion backscattering/channeling showed that this produced a highly defected, supersaturated solution with a peak concentration of 8 at.% at 35 nm. The specimen was then injected with 1.5×10^{16} D/cm^2 at 15 keV and a temperature of 90 K, and a retention-versus-temperature profile like that of Fig. 7 was measured. A control experiment was also performed in which Fe self-ions were implanted instead of the Y, thereby creating damage without altering the composition. Data from the two experiments are given in Fig. 9.

The profile for the self-ion-irradiated Fe is virtually unchanged from that obtained with D implantation alone (Fig. 7). Apparently, the number and character of defect traps are similar in the two cases. In contrast, the Fe layer implanted with Y retained most of the D to temperatures well above the

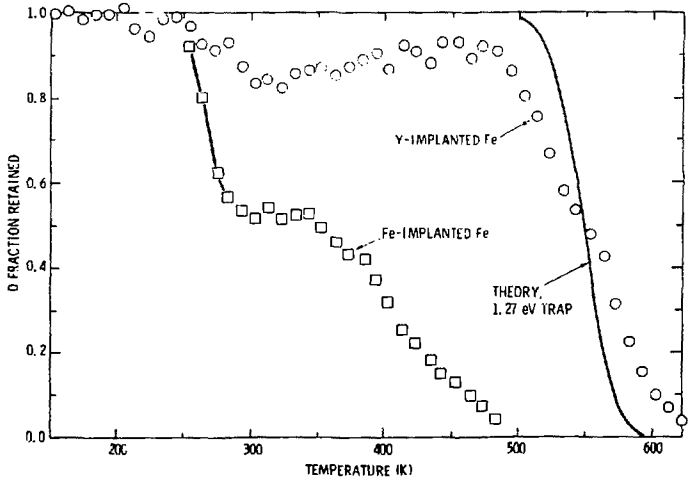

Fig. 9 – Release of D from traps in Y-implanted Fe and Fe-implanted Fe during linear ramping of temperature. The theoretical solid line assumes a unique trap depth of 1.27 eV.

two release stages observed in pure Fe; about 100% of the release occurred in an interval centered at ≈560 K. The time evolution of this system was modeled using Eqs. 2 - 5, assuming that one trap exists at each Y atom. A single trap enthalpy of $Q_1 = 1.27$ eV then yields the solid curve in Fig. 9. The width of the experimentally observed release stage is significantly greater than predicted by the calculation, suggesting an appreciable range of trap depths centered at ≈1.3 eV.

With regard to the mechanism of the above Y effect, it seems improbable that a coupling as strong as 1.3 eV results simply from a chemical interaction between substitutional Y and interstitial D. A more plausible hypothesis is that the oversize Y atom, whose elemental atomic volume is 2.8 times that of Fe, collects irradiation-induced vacancies to produce an impurity-stabilized defect. Evidence exists for such effects in both bcc and fcc lattices(16,17). The strong trapping may then reflect the combination of a Y-D chemical interaction and coupling to a lattice imperfection. Support for this interpretation comes from another experiment(7) in which the Fe host was implanted with Kr instead of Y. The inert-gas atom is also oversized in Fe, but it has no chemical affinity for hydrogen. In this case, the retention-versus-temperature profile for implanted D was qualitatively like that of Y-implanted Fe, with almost 100% of the release occurring in a single stage, but the release temperature was reduced by ≈80 K. The difference is tentatively attributed to the absence of a chemical component in the trapping.

Traps with a depth of 1.3 eV are potentially very useful for controlling hydrogen mobility in steels. They are virtually irreversible at room temperature, yet capable of being emptied by moderate annealing. In considering such applications, however, a key question is whether the responsible entities can be introduced by means other than ion implanation. The answer to this must await a more complete understanding of the mechanism.

In concluding this section on hydrogen trapping, it is instructive to consider the difference in experimental approach from that used to study Sb trapping by carbide precipitates. The hydrogen work entailed simply monitoring the decreasing quantity of trapped hydrogen during linear ramping of temperature, whereas in the Sb study both the trapped quantity and the concentration in solution were measured as a function of isothermal annealing. The latter method is actually the more sensitive to trapping, and it is particularly suitable when the trap depth is small compared to the activation enthalpy for diffusion. In the Fe-Sb-TiC system, these quantities are 0.4 eV and 2.8 eV respectively. For hydrogen in Fe, the situation is reversed, with trap depths $\geq$0.5 eV and a diffusion enthalpy of ≈0.05 eV. Under this condition, it is quite sufficient to monitor detrapping with increasing temperature. Moreover, the presence of a relatively strong trap may render the solutionized concentration too small to measure, as was the case in the hydrogen experiment.

Conclusion

Ion-implanted alloys provide a useful medium in which to identify and characterize impurity immobilization mechanisms. This is demonstrated by the variety of processes investigated in the present work, which exemplify each of the four principal ways in which solute transport can be reduced: incorporation into a stable intermetallic phase, and trapping by precipitates, other solutes, or lattice defects. In every case the implantation experiment either identified the process for the first time or substantially expanded knowledge of its properties. Since, additionally, the experimental approach and methods of data analysis used in this work are widely applicable, they provide a significant new capability for alloy development.

Acknowledgments

It is a pleasure to acknowledge the collaboration of J. E. Smugeresky in the Be work, that of D. M. Follstaedt and H. J. Rack in the study of Sb trapping, and that of S. T. Picraux and R. E. Stoltz in the hydrogen investigation. The technical assistance of C. T. Fuller was invaluable throughout.

References

1. Effect of Hydrogen on Behavior of Materials, A. W. Thompson and I. M. Bernstein, eds.; AIME, New York, 1976.

2. I. Olefjord, "Temper Embrittlement," International Metals Reviews, no.4 (1978) pp. 149-163.

3. S. M. Myers and J. E. Smugeresky, "Phase Equilibria and Diffusion in the Be-Al-Fe System Using High-Energy Ion Beams," Metall. Trans. A, 7 (1976) pp. 795-802.

4. S. M. Myers and J. E. Smugeresky, "Phase Equilibria in the Be-Al-Fe System Using High-Energy Ion Beams: II," Metall. Trans. A, 9 (1978) pp. 1789-1794.

5. S. M. Myers, D. M. Follstaedt, and H. J. Rack, "An Ion-Beam Study of Sb Trapping in Be-Ti-Sb-C Alloys," Appl. Phys. Lett., 33 (1978) pp. 396-398, and unpublished.

6. S. M. Myers, S. T. Picraux, and R. E. Stoltz, "Defect Trapping of Ion-Implanted Deuterium in Fe," J. Appl. Phys., 50 (1979) pp. 5710-5719.

7. S. M. Myers, S. T. Picraux, and R. E. Stoltz, unpublished.

8. S. H. Gelles, "Impurity Effects in Beryllium," Metals and Ceramics Information Center Report No. MCIC 72-06, 1972.

9. R. B. McLellan, "Thermodynamics of Solid Solutions," Mater. Sci. Eng., 9 (1972) pp. 121-140.

10. S. M. Myers and J. E. Smugeresky, "Low-Temperature Solubility of Copper in Beryllium, in Beryllium-Aluminum, and in Beryllium-Silicon Using Ion Beams," Metall. Trans. A, 8 (1977) pp. 609-616.

11. J. A. Borders and J. M. Harris, "The Use of $^{12}C(d,p)^{13}C$ and $^{16}O(d,p)^{17}O$ Reactions to Profile Carbon and Oxygen in Solids," Nucl. Instrum. Methods, 149 (1978) pp. 279-284.

12. A. McNabb and P. K. Foster, "A New Analysis of the Diffusion of Hydrogen in Iron and Ferritic Steels," Trans. AIME, 227 (1963) pp. 618-627.

13. F. S. Ham, "Theory of Diffusion-Limited Precipitation," J. Phys. Chem. Solids, 6 (1958) pp. 335-351.

14. S. M. Myers, D. E. Amos, and D. K. Brice, "Modeling of Enhanced Diffusion Under Ion Irradiation," J. Appl. Phys., 47 (1976) pp. 1812-1819.

15. A. J. Kumnick and H. H. Johnson, "Deep Trapping States for Hydrogen in Deformed Iron," Acta Metall. (1979), in press.

16. H. de Waard and L. C. Feldman, "Lattice Location of Impurities Implanted into Metals," pp. 317-351 in Applications of Ion Beams to Metals, S. T. Picraux, E. P. EerNisse, and F. L. Vook, eds.; Plenum, New York 1974.

17. A. S. Berger and R. W. Siegel, "Vacancy-Scandium Interaction in Quenched Copper," J. Phys. F, 9 (1979) pp. L67-L71.